

Article

Emergent scale invariance and climate sensitivity

Martin Rypdal^{1*}, Hege-Beate Fredriksen¹, Eirik Myrvoll-Nilsen¹, Kristoffer Rypdal¹ and Sigrunn H. Sørbye¹

¹ Department of Mathematics and Statistics, UiT The Arctic University of Norway, Norway

* Correspondence: martin.rypdal@uit.no; Tel.: +47-776-20754

Abstract: Earth's global surface temperature shows variability on an extended range of temporal scales and satisfies an emergent scaling symmetry. Recent studies indicate that scale invariance is not only a feature of the observed temperature fluctuations, but an inherent property of the temperature response to radiative forcing, and a principle that links the fast and slow climate responses. It provides a bridge between the decadal- and centennial-scale fluctuations in the instrumental temperature record, and the millennial-scale equilibration following perturbations in the radiative balance. In particular, the emergent scale invariance makes it possible to infer equilibrium climate sensitivity (ECS) from the observed relation between radiative forcing and global temperature in the instrumental era. This is verified in ensembles of Earth system models (ESMs), where the inferred values of ECS correlate strongly to estimates from idealized model runs. For the range of forcing data explored in this paper, the method gives best estimates of ECS between 2.3 and 3.4 K.

Keywords: Climate sensitivity; scale invariance; long-range persistence; climate variability; emergent constrains.

1. Introduction

The Intergovernmental Panel on Climate Change [1] (IPCC) has estimated the likely range of ECS to be between 1.5 and 4.5 K. The ECS, which is widely used in assessments of anthropogenic climate change, is defined as the asymptotic temperature increase following an instantaneous CO₂ doubling. In ESMs, the ECS is generally estimated via the so-called Gregory plots [2], where the response in the top-of-the-atmosphere radiation N is plotted against the global mean surface temperature anomaly ΔT during the equilibration following an instantaneous doubling or quadrupling of the atmospheric CO₂ concentration. The assumption is that the adjustment in radiation depends linearly on the surface temperature increase,

$$N = F - \lambda \Delta T, \quad (1)$$

so that the feedback parameter λ and the forcing F can be determined via linear regression. The ECS is hence $F_{2 \times \text{CO}_2} / \lambda$, where $F_{2 \times \text{CO}_2}$ is the forcing associated with a CO₂ doubling. The Gregory plots show that the linearity assumption is only approximate, and in particular, there are slow feedbacks in the models that reduce the feedback parameter as the planet warms [3]. A state dependence is also observed in the so-called paleo sensitivity [4–7]. Nevertheless, the usefulness of ECS and its estimation still relies on the linearity assumption in Equation 1. Satellite observations of the top-of-the-atmosphere radiation are available through the Clouds and the Earth's Radiant Energy System (CERES), but unfortunately, the data only covers the years 2000-present. The state-of-the-art ECS estimates based on the satellite data gives a wide likely range (in this case a 17-83% confidence interval) of 2.4-4.5 K [8].

A different approach, which can be used when the top-of-the-atmosphere radiation is unknown, is to combine model results with the instrumental temperature record. Recently Cox et al. claimed that ECS can be constrained to a "likely range" (in this paper specified to be the 66% confidence

interval) of 2.2 to 3.4 K, with a best estimate of 2.8 K [9]. They propose a metric in both the instrumental temperature record in the period 1880 to 2016 and in the corresponding historical runs in the Coupled Model Intercomparison Project Phases 5 (CMIP5) ensemble. By exploring a so-called emergent relationship, they estimate a distribution for the Gregory estimate of ECS conditioned on their proposed metric, and using the law of total probability in conjunction with Bayes Theorem they obtain a probability density function for the ECS when it is constrained by the instrumental record. However, it has been demonstrated that their estimated metric depends on the response to the strong anthropogenic forcing in the time period after year 1950, and hence one has to take into account that models in the ensemble are forced differently [10].

A more consistent method of constraining ECS from the instrumental record is to include data for historical forcing, with its uncertainties, and to estimate response functions that describe the relationship between global radiative forcing and the global surface temperature. If one adopts a hypothesis of a linear and stationary response, then the temperature anomaly ΔT can be written as a convolution of the forcing F with a response function $G(t)$:

$$\Delta T(t) = \int_{-\infty}^t G(t-s) \left(F(s) ds + dB(s) \right), \quad (2)$$

where the term $F(t)$ is the known (deterministic) forcing and $dB(t)$ represents a white-noise random forcing that gives rise to the internal variability. As discussed in Section 2, such a linear response can arise naturally from a multi-layer energy balance model, where the response function is a sum of exponential functions with decay rates that are given by the real and negative eigenvalues of the system of differential equations. Fredriksen and Rypdal [11] have shown that three exponential terms are sufficient to obtain a model that simultaneously displays responses to historical and reconstructed forcings that are consistent with the instrumental temperature record and the reconstructed last millennium global mean temperature, respectively. In addition, it correctly describes the statistical properties of the internal variability on time scales from months to centuries. The constructed response function corresponds to an ECS estimate of 3.0 K, obtained via the formula

$$\text{ECS} = F_{2 \times \text{CO}_2} \int_0^{\infty} G(t) dt. \quad (3)$$

The forcing $F_{2 \times \text{CO}_2}$ is well approximated by a logarithmic dependence of the CO_2 concentration, with a best estimate of 3.7 W/m^2 found by the IPCC [1]. Uncertainties associated with the radiative transfer calculations are small [12]. However, forcing estimates from CMIP5 models often include rapid adjustments of the atmosphere, resulting in larger uncertainties [13]. The more serious issues are the uncertainty in the estimate of the response function, the uncertainty in the forcing data, and the validity of the linearity assumption.

The uncertainty in the response function estimates can be assessed in several ways, for instance using an ensemble of runs of the same experiment in one ESM. The uncertainty in the forcing presents a significant challenge, which is not addressed by Cox *et al.* [9]. In this paper, we take part of this uncertainty into account by analyzing the spread in the adjusted forcing over the CMIP5 ensemble. In historical model runs the adjusted forcing is obtained from Equation 1 by comparing the time series of $\Delta T(t)$ and the top-of-the-atmosphere radiation $N(t)$ for a fixed estimate of the feedback parameter λ [14]. The resulting time series $F(t)$ is an estimate of the forcing experienced by the ESM. However, the construction of $F(t)$ from the assumed linear relationship between $\Delta T(t)$ and $N(t)$ results in forcing signals where some short-scale internal climate variability, including the El Niño Southern Oscillation (ENSO), are clearly observable in the forcing signal. Consequently, these forcing data are not suitable for statistical estimation of response functions $G(t)$ from Equation 2. The alternative, which is used in this paper, is to fix a forcing time series, for instance the time series provided by Hansen *et al.* [15], and to modify it for each model so that the trend (or low-frequency variability) is equal to the adjusted forcing for the model. This approach serves two purposes. First, we ensure that when we

fit a response function to a model, the increasing trend in the forcing is consistent with the forcing in the model run. Secondly, this provides an ensemble of forcing time series with different trends. The estimates of the response function from the observational temperature record can be repeated across this ensemble of forcing time series and provide an estimate of the uncertainty in the response functions that is associated with the uncertainty in the forcing trend.

It is now natural to assume a general form of the response function, i.e.

$$G(t) = \sum_{k=1}^N c_k e^{-t/\tau_k}, \quad (4)$$

and to obtain estimates \hat{c}_k and $\hat{\tau}_k$ from historical runs of each of the ESMs in the CMIP5 ensemble, as well as for the instrumental temperature record. For each model, this estimate corresponds to an estimate of ECS through Equation 3, which in this case reads

$$\widehat{\text{ECS}} = F_{2 \times \text{CO}_2} \sum_{k=1}^N \hat{c}_k \hat{\tau}_k.$$

If the estimate $\widehat{\text{ECS}}$ correlates strongly with the Gregory estimate of ECS over the CMIP5 ensemble, then the estimate $\widehat{\text{ECS}}$ obtained from the instrumental temperature record can be used to constrain the distribution of ECS in the ensemble. Unfortunately, such an analysis will show a very weak correlation between the two estimates, and this apparently indicates that response function estimates are useless for constraining ECS. On the other hand, the reason for the low correlation is that the instrumental temperature record is too short to provide any information about the slow response of the climate system, and the general form of the response function leads to statistical overfitting. The method can be improved by reducing the number of free parameters. The naïve approach, which is to reduce the response function to one characteristic time scale, gives a model that is unable to accurately describe the temporal structure of the temperature response, and would lead to a systematic underestimation of the ECS. A better alternative is to use the emergent property of temporal scale invariance.

Rypdal and Rypdal [16] have demonstrated that a scale-invariant response model, i.e. Equation 2 with

$$G(t) = \left(\frac{t}{\mu}\right)^{\beta/2-1} \Theta(t) \zeta, \quad (5)$$

(where $\zeta = 1 \text{ km}^2 \text{ J}^{-1}$ is a factor needed to give $G(t)$ the right physical dimension and $\Theta(t)$ is the unit-step function), provides a parsimonious and accurate model on time scales from months to centuries. This is in spite of the fact that energy is not conserved in the model, and that the ECS according to Equation 3 is infinite. The reason why this is possible is that the temperature records and the forcing time series we have for the industrial period are relatively short compared to the time it takes for global surface temperature to adjust after an abrupt CO_2 doubling in ESMs. This also explains why it is so difficult to provide accurate estimates of ECS from observational data; the fact that a model with infinite ECS can perform well when tested on observational data indicate that these time series are too short for ECS assessment. As a consequence it is natural to conclude that ECS is not the most useful measure of climate sensitivity in the face of anthropogenic climate change, and that it may be more useful to study a scale-dependent (or frequency-dependent) sensitivity defined as

$$R(f) = F_{2 \times \text{CO}_2} |\hat{G}(f)|, \quad (6)$$

where

$$\hat{G}(f) = \int_{-\infty}^{\infty} G(t) e^{-2\pi i f t} dt$$

is the Fourier transform of the response function. However, as the main results of this paper will show, the scale dependent sensitivity evaluated at $f = 10^{-3} \text{ yrs}^{-1}$ correlates strongly with the Gregory estimate of ECS. Hence, this technique can be used to constrain the ECS in the model ensemble on the instrumental temperature record. It is evident from the results presented in this paper that uncertainty in the historical forcing data is the main obstacle for more accurate assessment of ECS.

The paper is structured as follows. In section 2 we discuss stochastic linear response models for global surface temperature variability to motivate the analyses presented in this paper. We also discuss some dissipation-response relations that follow from this modeling framework. In section 3 we present the main results, and in section 4 we discuss and conclude our findings. Details on the statistical analyses are presented in section 5.

2. Linear response models and scale-dependent sensitivity

2.1. The 1-box energy balance model

The simplest climate model, the so-called 1-box energy balance model, describes the temperature anomaly ΔT via the first order differential equation

$$Cd\Delta T(t) = -\lambda\Delta Tdt + F(t)dt,$$

where C is a heat capacity, λ is the feedback parameter and $F(t)$ is the radiative forcing. If one includes a white-noise stochastic forcing, the model becomes a stochastic differential equation on the form

$$Cd\Delta T(t) = -\lambda\Delta Tdt + F(t)dt + \sigma dB(t), \quad (7)$$

where $dB(t)$ is the white-noise random measure. The solution of the equation is

$$\Delta T(t) = \frac{1}{C} \int_{-\infty}^t e^{-(t-s)/\tau} F(s)ds + \frac{\sigma}{C} \int_{-\infty}^t e^{-(t-s)/\tau} dB(s), \quad (8)$$

where the characteristic time scale is $\tau = C/\lambda$. The second term in the above expression defines the Ornstein-Uhlenbeck process

$$X(t) = \frac{\sigma}{C} \int_{-\infty}^t e^{-(t-s)/\tau} dB(s),$$

i.e. the continuous-time version of an AR(1) process, sometimes referred to as red noise. This is a Gaussian process characterized by its exponentially decaying correlation function. In fact, the covariance structure of the process is given by the expression

$$r_X(\Delta t) = \langle X(t)X(t + \Delta t) \rangle = \frac{\sigma^2\tau}{2C^2} e^{-|\Delta t|/\tau},$$

and from the Wiener-Kinchin theorem it follows that the power-spectral density (PSD) of $X(t)$ is Lorentzian

$$S_X(f) = \int_{-\infty}^{\infty} r_X(t) e^{-2\pi i f t} dt = \frac{1}{C^2} \frac{\sigma^2\tau^2}{1 + 4\pi^2\tau^2 f^2}.$$

The PSD scales as $S(f) \sim f^{-2}$ for frequencies $f \gg 1/\tau$, and as $S(f) \approx \sigma^2\tau^2/C^2$ for $f \ll 1/\tau$.

The first term in Equation 8 can be referred to as the response to the deterministic (or known) forcing, and denoted $\Delta T_{\text{det}}(t)$. If the forcing is an instantaneous CO_2 doubling at time $t = 0$ we can write $F(t) = F_{2\times\text{CO}_2}\Theta(t)$, where $F_{2\times\text{CO}_2}$ is the forcing corresponding to the CO_2 doubling, and $\Theta(t)$ is the unit-step function. The response is

$$\Delta T_{\text{det}}(t) = \frac{F_{2\times\text{CO}_2}}{C} \int_0^t e^{-(t-s)/\tau} ds = \frac{F_{2\times\text{CO}_2}\tau}{C} (1 - e^{-t/\tau}).$$

In particular an expression for the ECS is obtained in the limit $t \rightarrow \infty$:

$$\text{ECS} = \frac{F_{2 \times \text{CO}_2} \tau}{C} = \frac{F_{2 \times \text{CO}_2}}{\lambda}.$$

We note that there are connections between the response to deterministic forcing and the statistical properties of the random fluctuations $X(t)$. For instance, the low-frequency limit of the PSD is proportional to the square of the ECS:

$$\lim_{f \rightarrow 0} S_X(f) = \int_{-\infty}^{\infty} r_X(t) dt = \frac{\sigma^2 \tau^2}{C^2} = \frac{\sigma^2}{\lambda^2} = \frac{\sigma^2}{F_{2 \times \text{CO}_2}^2} \text{ECS}^2.$$

The above expression is an example of a dissipation-response relation that holds for more general linear response models.

2.2. Generalizations of the 1-box model

The 1-box energy-balance model describes temperature response through a single characteristic time scale, and does not accurately take into account the warming of the deep oceans, which is much slower than the thermal response of the atmosphere. A more accurate energy-balance model is the so-called 2-box model, for which the analog of Equation 7 is

$$\begin{aligned} C_1 d\Delta T_1(t) &= -\lambda \Delta T_1 dt + \kappa (\Delta T_2 - \Delta T_1) dt + F(t) dt + \sigma dB(t) \\ C_2 d\Delta T_2(t) &= -\kappa (\Delta T_2 - \Delta T_1) dt. \end{aligned}$$

For $\kappa > 0$, this system has two negative eigenvalues $-1/\tau_1$ and $-1/\tau_2$, and the surface temperature anomaly $\Delta T = \Delta T_1$ can be written as Equation 2, where $G(t) = (c_1 e^{-t/\tau_1} + c_2 e^{-t/\tau_2}) \Theta(t)$ now is a response function with two characteristic time scales. The model can be further generalized to the class of N -box models for which we have a response function given by Equation 4, or to an even more general class of models for which we just assume that there is some response function $G(t)$ with $G(t) = 0$ for $t < 0$. In the general case we have

$$r_X(\Delta t) = \langle X(t) X(t + \Delta t) \rangle = \sigma^2 \int_0^{\infty} G(t) G(t + \Delta t) dt$$

for $\Delta t > 0$, and from Equation 3 (which holds in general) it follows that

$$\text{ECS}^2 = F_{2 \times \text{CO}_2}^2 \int_0^{\infty} \int_0^{\infty} G(t) G(s) dt ds = \frac{F_{2 \times \text{CO}_2}^2}{\sigma^2} \int_{-\infty}^{\infty} r_X(\Delta t) d\Delta t = \frac{F_{2 \times \text{CO}_2}^2}{\sigma^2} \lim_{f \rightarrow 0} S_X(f). \quad (9)$$

2.3. Scale-invariant models

The statistical properties of global surface temperature are consistent with those of long-range dependent (LRD) stochastic properties [17–22], in particular with fractional Gaussian noise (fGn). This can be modeled by letting the response function $G(t)$ take the form of Equation 5. In fact, the stochastic component

$$X(t) = \int_{-\infty}^t \left(\frac{t-s}{\mu} \right)^{\beta/2-1} \zeta dB(s)$$

can be taken as a formal definition of a fGn (see the Appendix of [16]). Its PSD is $S(f) \sim f^{-\beta}$. Studies also indicate that scale invariance is not only a feature of the observed temperature fluctuations, but

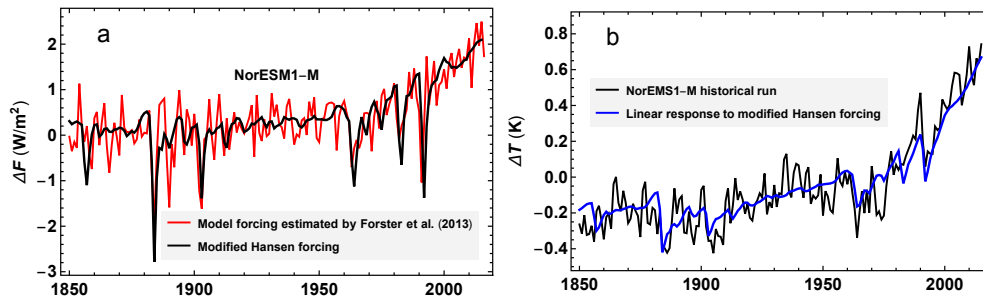


Figure 1. (a) The red curve is the adjusted forcing for the NorESM1-M model provided by Forster *et al.* [14]. The black curve is the forcing data of Hansen *et al.* [15] modified so that its 17-yr moving average equals the 17-yr moving average of the red curve. (b) The black curve is the global surface temperature in the historical run of the NorESM1-M model, and the blue curve is the response to the modified Hansen forcing (the black curve in (a)) for the model given by Equation 5. Parameters are estimated as $\beta = 0.67$ and $\mu = 7.8 \times 10^{-3} \text{ yrs}^{-1}$.

an inherent property of the temperature response to radiative forcing [11,16,22–24]. This means that the deterministic component

$$\Delta T_{\text{det}}(t) = \int_{-\infty}^t \left(\frac{t-s}{\mu} \right)^{\beta/2-1} F(s) \zeta ds$$

is an accurate description of the temperature response to the known deterministic forcing. Moreover, the stochastic and deterministic responses can simultaneously describe the deterministic temperature response and the climate noise (residual), meaning that the parameters β and μ can take the same values in the two terms. This is a type of dissipation-fluctuation result, but not as strong as those that directly link the statistical properties of the climate noise to the characteristics of the response. More importantly, it provides a statistical model for which parameter estimates are very stable, and this makes these models suitable for extracting proxies of ECS from historical runs in the model ensemble.

3. Results

For each ESM in the CMIP5 ensemble we take the adjusted forcing provided by Forster *et al.* [14] and modify the forcing data of Hansen *et al.* [15] so that the 17-yr moving averages of the two time series are equal. For the model given by Equation 2 with response function given by Equation 5 we fit parameters β and μ to the global surface temperature of the historical run of the given ESM, using the modified Hansen forcing as input. The parameters are estimated using a technique described in section 5. Figure 1(a) shows the adjusted forcing and the modified Hansen forcing for the NorESM1-M model, and Figure 1(b) shows the response to the modified Hansen forcing according to the fitted linear response model together with the global surface temperature in the historical run of the NorESM1-M model.

When parameters β and μ are estimated for the historical runs of each ESM, the estimated scale dependent sensitivity $R(f)$ can be computed for each model using Equation 6. The factor $F_{2 \times \text{CO}_2}$ is taken individually for each model based on the Gregory estimates in [1]. A scalar metric R is obtained by evaluating the functions $R(f)$ at the frequency $f = 10^{-3} \text{ yrs}^{-1}$. The results are presented in Table 1. The choice of frequency is based on how well the corresponding scalar metric correlates with the Gregory estimates of ECS. Figure 2(a) shows that over the model ensemble, $R(f)$ typically equals the Gregory estimate of ECS for frequencies $f \approx 10^{-3} \text{ yrs}^{-1}$, and Figure 2(b) shows that the correlation (over the model ensemble) between $R(f)$ and the Gregory estimate of ECS has its maximum for $f \approx 10^{-3} \text{ yrs}^{-1}$.

Figure 3(a) shows a plot of the R , i.e. $R(f)$ evaluated at $f = 10^{-3} \text{ yrs}^{-1}$, versus the Gregory estimate of ECS. The points (letters) represent the different ESMs in the model ensemble, and the

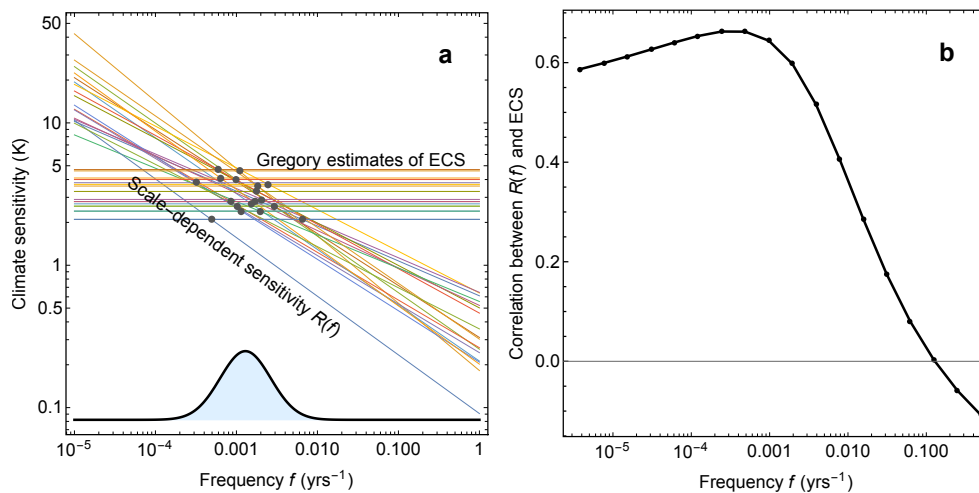


Figure 2. (a) A double-logarithmic plot of the scale dependent sensitivity $R(f)$ for each ESM in the ensemble. The scale-dependent sensitivities are computed from Equation 6 under the assumption that the response function is scaling and given by Equation 5. Hence the $R(f)$ -curves are power-laws and displayed as straight lines in the double-logarithmic plot. The different slopes correspond to different β -estimates. The horizontal lines indicate the ECS of the ESMs obtained from the Gregory plots and reported in [1], and the black dots indicate for which frequency f we have $R(f) = \text{ECS}$ for each model. (b) Shows the correlation (over the ensemble of ESMs) between the scale-dependent sensitivity $R(f)$ and the Gregory estimate of the ECS. The correlation coefficient is plotted as a function of the frequency f , and shows a maximum at $f \approx 10^{-3} \text{ yrs}^{-1}$.

contour plot shows the conditional probability density function (PDF) $p(\text{ECS}|R)$ estimated from the seventeen data points corresponding to the seventeen ESMs in the ensemble. The method used to estimate $p(\text{ECS}|R)$ is identical to the one described in [9].

The vertical black line in Figure 3(a) is $R = 2.9 \text{ K}$. This value of R is obtained from the parameters $\beta = 0.66$ and $\mu = 11.9 \times 10^{-3} \text{ yrs}^{-1}$, which are estimated from the instrumental temperature record using the Hansen-forcing. We have used $F_{2 \times \text{CO}_2} = 3.8 \text{ W/m}^2$, which is the value for the GISS-E2-R model. The black curve in the lower part of Figure 3(a) is an estimated PDF $P(R)$ for the metric R . The pdf is obtained by considering two sources of uncertainty in the R -estimates. The first is the spread in parameter estimates when we vary the forcing. The forcing is varied over the set of modified Hansen forcing time series, where each modification corresponds to a historical run of a ESM in the ensemble. The parameter estimates for the instrumental temperature record, and the resulting value of R , for varying forcing data is shown in Table 2. The second is the spread in the parameters β and μ across repeated historical runs of the same model, i.e. runs where the known forcing is the same, but where we due to chaotic dynamics have random components that vary between realizations. Table 3 shows a set of parameter estimates for repeated historical runs of the CSIRO model. The total variability from these two sources is obtained by a simple mixture model, and the plotted PDF is computed by a smooth kernel method. The black curve in Figure 3(b) shows the PDF for ECS computed from the formula

$$p(\text{ECS}) = \int p(\text{ECS}|R)p(R)dR, \quad (10)$$

where $p(R)$ is the PDF shown in 3(a). The histogram in Figure 3(b) is the distribution of ECS in the model ensemble, and the dotted curve in Figure 3(b) is a Gaussian fit to the distribution of ECS in the model ensemble. The figure demonstrates that when constrained by the scale-dependent sensitivity of the instrumental temperature record, the best estimate of ECS in the model ensemble is reduced by approximately 0.2 K. The pdf $p(R)$ shown in Figure 3a, also shows that, with the uncertainties taken

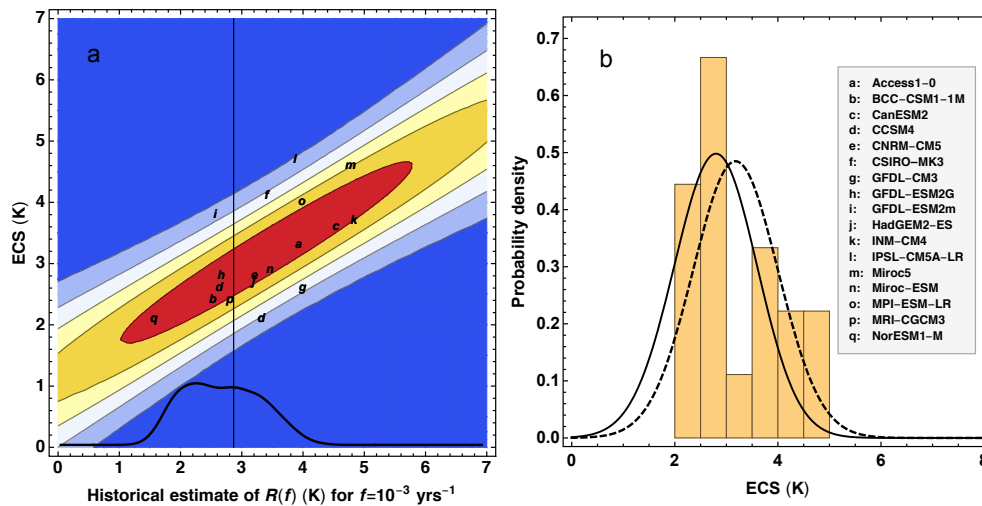


Figure 3. (a) Shows a plot of the R , i.e. $R(f)$ evaluated at $f = 10^{-3} \text{ yrs}^{-1}$, versus the Gregory estimate of ECS. The points (letters) represent the different ESMs in the model ensemble, and the contour plot shows the conditional probability density function (PDF) $p(\text{ECS}|R)$. The vertical black line in Figure 3(a) is $R = 2.9 \text{ K}$. This value of R is obtained from the parameters $\beta = 0.66$ and $\mu = 11.9 \times 10^{-3} \text{ yrs}^{-1}$, which are estimated from the instrumental temperature record using the Hansen forcing. The thick, black curve is the estimated PDF of $R(f)$. (b) The full curve in Figure 3(b) shows the PDF for ECS computed from the Equation 10, where $p(R)$ is the PDF shown in 3(a). The histogram in Figure 3(b) is the distribution of ECS in the model ensemble, and the dotted curve in in Figure 3(b) is a Gaussian fit to the histogram.

into account in this work, models with ECS larger than 4 K are inconsistent with the instrumental temperature record.

The results of this paper can alternatively be presented without estimating a conditional PDF. From the scatter plot in Figure 3(a) we can fit a linear relationship between R and ECS, and in Table 2 we have a set of estimates of R for the instrumental temperature record. The linear fit maps each of the R -estimates to an ECS-value, which can be interpreted as the best estimate of ECS based on the corresponding forcing data. This mapping is shown in Figure 4(a). The range of these best estimates of ECS are between 2.3 and 3.4 K. A histogram of the best estimates is shown in Figure 4(b).

4. Discussion

The PDF for the ECS shown in Figure 3(b) is similar to the one presented by Cox *et al.* [9]. However, there are important differences in methodology that must be pointed out. Cox *et al.* use a pure dissipation-response relationship to constrain ECS in the model ensemble. They propose a metric Ψ , which is analogous to the metric R proposed in this work, and claim that estimates of Ψ are independent of the forcing. This claim has been demonstrated to be false [10]. In our framework, an approach in the spirit of Cox *et al.* would be to use Equation 9, and to seek estimates of the correlation function (or equivalently the PSD) of the climate noise $X(t)$ that are independent of the forcing. Such an approach would lead to the same problems as those in [9], namely that the estimates would be influenced by the strong anthropogenic forcing in the instrumental period. This is our motivation for developing a method that employs forcing data in the estimation of our metric R , and as a consequence we have to take the uncertainty in the forcing into account. We have done this by using a fixed data set for historical forcing (the Hansen-forcing) and varied its low-frequency variability over the ensemble of adjusted forcing time series provided by Forster *et al.* [14]. Clearly, this does not represent the full uncertainty in the historical forcing, and hence the spread in the distribution of ECS (the black curve in Figure 3(b)) is narrower than what we expect to find if we were to model the full

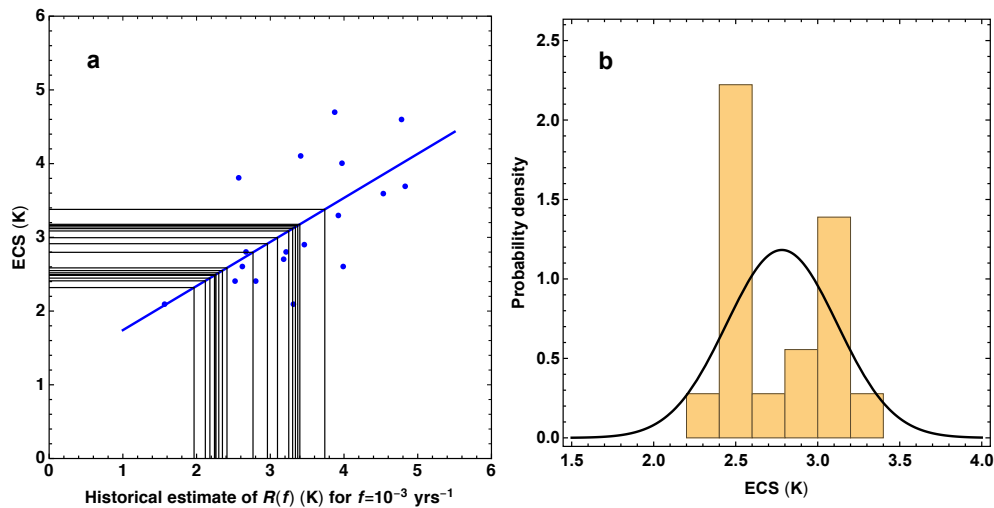


Figure 4. (a) The points in the scatter plot are the same as (the letters) in Figure 3(a). The blue line is the least-square fit of the model $ECS = aR + b$. The vertical lines correspond to the R -values estimated from the instrumental temperature record for the different modified Hansen forcing time series. The horizontal lines show how these R -values are mapped to ECS-values by the linear relation $ECS = aR + b$. (b) Shows a histogram of the ECS-values that are displayed as horizontal lines in (a). The black curve is a Gaussian fit to the histogram.

forcing uncertainty. We conclude that accurate estimates of the uncertainty in historical forcing is a key for establishing constraints on ECS in ESM ensembles. The modeling of the relationship between R and ECS is also a source of uncertainty. It is evident from Figure 4(a) that the coefficient a in the linear map $ECS = aR + b$ is less than one. In fact, its estimated value is $a = 0.6$. As a consequence the mapping from R to ECS is contracting, so that the spread in ECS-values is smaller than the spread in R -values. The same is true for the analysis presented in Figure 3, since the conditional PDF $p(ECS|R)$ is constructed from the fitted line $ECS = aR + b$. We note that for a model without the intercept term b , the estimated coefficient is $a = 0.91$, and the range of the best estimates of ECS becomes 1.8 – 3.4 K. Other assumptions about the functional relationship between R and ECS will lead to yet different ranges of best estimates.

Apart from the constraints on ECS, an important result presented in this paper is that scale-dependent climate sensitivity provides a good proxy for ECS. Moreover, despite having infinite ECS, scale-invariant linear response models are useful for estimating ECS from observational data. The advantage over multi-layer energy balance models is that the scale-invariant models have few free parameters and are not prone to statistical overfitting. The accuracy of the models is associated with the scaling nature of climate variability, an emergent property of the complex climate system.

5. Materials and Methods

5.1. Data

The instrumental temperature record used in this paper is the HadCRUT4 observational dataset which was downloaded from <https://crudata.uea.ac.uk/cru/data/temperature/>. The CMIP5 ESM data was downloaded from <https://esgf-data.dkrz.de/search/cmip5-dkrz/>. Forcing data was retrieved from the sources provided in [15] and [14]. The time period 1850-2016 is used for all historical runs and for the instrumental temperature record.

Table 1. Shows estimated quantities for the ESM in the ensemble. The columns for ECS and $F_{2\times\text{CO}_2}$ are obtained from Gregory plots for $4\times\text{CO}_2$ runs and taken from [1]. The columns denoted β , μ and σ show the estimates of the parameters in the model given by Equation 2 with response function given by Equation 5, obtained from historical runs of the ESMs and the modified Hansen forcing for each model. The last column displays the scale-dependent sensitivity $R(f)$ obtained from Equation 6 using the values of $F_{2\times\text{CO}_2}$, β and μ that are listed in the columns to the left, and evaluated at $f = 10^{-3}$ yrs $^{-1}$.

Model	ECS (K)	$F_{2\times\text{CO}_2}$ (W/m 2)	β	μ (10 $^{-3}$ yrs)	σ (W/m 2)	R (K)*
GISS-E2-R	2.1	3.8	0.49	13.8	0.07	3.3
HadGEM2-ES	4.6	2.9	0.95	7.3	0.32	4.8
IPSL-CM5A-LR	2.6	3.1	0.79	9.6	0.16	4.0
NorESM1-M	2.8	3.1	0.67	7.8	0.12	2.7
Access1-0	3.8	3.0	0.68	7.3	0.10	2.6
Miroc-ESM	4.7	4.3	0.73	6.6	0.12	3.9
Miroc5	2.7	4.1	0.78	4.0	0.21	3.2
CanESM2	3.7	4.1	0.59	17.5	0.15	4.8
CCSM4	2.9	3.8	0.49	14.9	0.12	3.5
CNRM-CM5	3.3	3.6	0.60	15.0	0.12	3.9
GFDL-CM3	4.0	3.0	0.62	19.0	0.14	4.0
GFDL-ESM2G	2.4	3.1	0.72	5.8	0.15	2.5
CSIRO-MK3	4.1	2.6	0.82	8.9	0.17	3.4
BCC-CSM1-1M	2.8	3.2	0.53	15.8	0.09	3.2
GFDL-ESM2m	2.4	3.1	0.47	15.3	0.16	2.8
INM-CM4	2.1	3.0	0.82	1.6	0.12	1.6
MPI-ESM-LR	3.6	4.1	0.78	7.6	0.16	4.5
MRI-CGCM3	2.6	3.2	0.58	9.9	0.10	2.6

*In the last column $R = R(f)$ for $f = 10^{-3}$ yrs $^{-1}$.

5.2. Parameter estimation

In discrete time, the statistical model given by Equations 2 and 5 can be written as

$$\Delta\mathbf{T} = \sigma_f G(\beta) (F_0 + \mathbf{F}) + \boldsymbol{\epsilon}(\sigma, \beta), \quad (11)$$

where we have defined a matrix

$$G_{t,s}(\beta) = \begin{cases} (t-s+\frac{1}{2})^{\beta/2-1}, & 1 \leq s \leq t \\ 0, & \text{otherwise} \end{cases}.$$

Here $\Delta\mathbf{T} = (\Delta T(t_1), \Delta T(t_2), \dots, \Delta T(t_n))^T$ is the time series for global surface temperature, $\mathbf{F} = (F(t_1), F(t_2), \dots, F(t_n))^T$ is the time series for the known forcing, and $\boldsymbol{\epsilon} = \boldsymbol{\epsilon}(\sigma, \beta) = (\epsilon(t_1), \epsilon(t_2), \dots, \epsilon(t_n))^T$, where $\boldsymbol{\epsilon}$ is a fGn with parameters β and σ . In this paper we only consider time series that are sampled yearly, so we let $t_i = i$, and omit the time unit for simplicity. The random vector $\boldsymbol{\epsilon}$ is a segment of a fGn, so by definition it is a stationary zero-mean Gaussian vector with covariance matrix

$$\Sigma_{i,j} = \frac{\sigma^2}{2} \left(|i-j+1|^{\beta+1} + |i-j-1|^{\beta+1} - 2|i-j|^{\beta+1} \right).$$

The parameter β is related to the Hurst exponent H through the relation $\beta = 2H - 1$ [25].

In fitting Equation 11 to a given temperature series, the parameters β , σ_f , σ and F_0 are found numerically using the methodology of integrated nested Laplace approximation (INLA) [26]. In addition, the parameter μ is determined using the formula $(1/\mu)^{\beta/2-1} = \sigma_f$. INLA is available within the programming environment R, using the open-source package R-INLA which can be downloaded from www.r-inla.org. It represents a computationally efficient Bayesian approach which gives

Table 2. The parameter estimates for the instrumental temperature record, and the resulting values of R , for varying forcing data.

Forcing	β	μ (10^{-3} yrs)	σ (W/m^2)	R (K)*
GISS-E2-R	0.61	5.8	0.12	2.4
HadGEM2-ES	0.87	5.3	0.20	3.3
IPSL-CM5A-LR	0.64	6.4	0.12	2.2
NorESM1-M	0.74	6.3	0.14	2.8
Access1-0	0.67	6.3	0.12	2.3
Miroc-ESM	0.68	7.6	0.14	3.7
Miroc5	0.68	6.6	0.12	3.3
CanESM2	0.68	5.5	0.13	3.0
CCSM4	0.62	4.5	0.13	2.1
CNRM-CM5	0.69	8.2	0.13	3.3
GFDL-CM3	0.86	5.6	0.19	3.4
GFDL-ESM2G	0.75	4.4	0.14	2.3
CSIRO-MK3	0.86	6.0	0.19	3.1
BCC-CSM1-1M	0.70	3.9	0.13	2.0
GFDL-ESM2m	0.73	4.9	0.14	2.4
INM-CM4	0.67	5.9	0.12	2.2
MPI-ESM-LR	0.81	1.8	0.15	2.3
MRI-CGCM3	0.79	6.9	0.15	3.4

*In the last column $R = R(f)$ for $f = 10^{-3}$ yrs $^{-1}$.**Table 3.** Shows a set of parameter estimates for repeated historical runs of the CSIRO model.

Ensemble run	β	μ (10^{-3} yrs)	σ (W/m^2)	R (K)*
1	0.82	13.0	0.17	3.5
2	0.91	8.0	0.23	3.9
3	0.80	19.4	0.16	4.1
4	0.88	13.6	0.23	4.4
5	0.73	21.8	0.14	3.6
6	0.89	9.9	0.22	3.8
7	0.82	16.9	0.17	4.1
8	0.87	9.5	0.19	3.4
9	0.86	11.6	0.19	3.8

*In the last column $R = R(f)$ for $f = 10^{-3}$ yrs $^{-1}$.

accurate estimates of the posterior marginals for all the parameters in Equation 11, potentially also including the predictor itself.

Specifically, INLA is designed to provide inference for a flexible class of three-stage hierarchical models, referred to as latent Gaussian models [26]. The first stage specifies that the observations (ΔT) are assumed conditionally independent given a latent field and hyperparameters. The second stage assumes that the latent field ($E(\Delta T)^T, \epsilon^T$) given additional hyperparameters is a zero-mean Gaussian Markov random field. This assumption implies that the precision (inverse covariance) matrix of the latent field will be sparse. The third stage specifies a prior for each of the hyperparameters ($\beta, \sigma, \sigma_f, F_0$).

The model defined by Equation 11 does not fit into the class of latent Gaussian models without modifications. First, the LRD properties of the fGn process make the precision matrix of the latent field dense. To ensure computational efficiency, this is circumvented by approximating the fGn as a weighted sum of four AR(1) processes as introduced in [27]. Second, the mean of the observation vector, $E(\Delta T) = \sigma_f G(\beta) \mathbf{F}$ has a non-standard form. This requires separate specification as described in [28], also providing implementation of the model using the freely available R package `INLA.climate`.

Author Contributions: All authors conceived and designed the study; H.F. collected data and constructed the modified forcing data. E.M.N. and S.H.S. performed the parameter estimates; M.R. and H.F. analyzed the results; M.R. wrote the paper with input from all authors.

Conflicts of Interest: The authors declare no conflict of interest.

Abbreviations

The following abbreviations are used in this manuscript:

ECS: Equilibrium climate sensitivity
 ESM: Earth system model
 IPCC: Intergovernmental Panel on Climate Change
 CERES: Clouds and Earth's Radiant Energy System
 CMIP5: Coupled Model Intercomparison Project Phase 5
 ENSO: El Niño Southern Oscillation
 PSD: Power Spectral Density
 LRD: Long-range dependence
 fGn: fractional Gaussian noise
 PDF: Probability density function
 INLA: Integrated nested Laplace approximation

References

1. IPCC. *Climate Change 2013: The Physical Science Basis. Contribution of Working Group I to the Fifth Assessment Report of the Intergovernmental Panel on Climate Change*; Cambridge University Press, 2013.
2. Gregory, J.M.; Ingram, W.J.; Palmer, M.A.; Jones, G.S.; Stott, P.A.; Thorpe, R.B.; Lowe, J.A.; Johns, T.C.; Williams, K.D. A new method for diagnosing radiative forcing and climate sensitivity. *Geophysical Research Letters* **2004**, *31*, L03205.
3. Knutti, R.; Rugenstein, M.A.; Hegerl, G.C. Beyond equilibrium climate sensitivity. *Nature Geoscience* **2017**, *10*, 727–736.
4. von der Heydt, A.S.; Köhler, P.; van de Wal, P.R.S.W.; Dijkstra, H.A. On the state dependency of fast feedback processes in (paleo) climate sensitivity. *Geophysical Research Letters* **2014**, *41*, 6484–6492.
5. von der Heydt, A.S.; Dijkstra, H.A.; van de Wal, R.S.W.; Caballero, R.; Crucifix, M.; Foster, G.L.; Huber, M.; Köhler, P.; Rohling, E.; Valdes, P.J.; Ashwin, P.; Bathiany, S.; Berends, T.; van Bree, L.G.J.; Ditlevsen, P.; Ghil, M.; Haywood, A.M.; Katzav, J.; Lohmann, G.; Lohmann, J.; Lucarini, V.; Marzocchi, A.; Pälike, H.; Baroni, I.R.; Simon, D.; Sluijs, A.; Stap, L.B.; Tantet, A.; Viebahn, J.; Ziegler, M. Lessons on Climate Sensitivity From Past Climate Changes. *Current Climate Change Reports* **2016**, *2*, 148–158.
6. von der Heydt, A.S.; Ashwin, P. State dependence of climate sensitivity: attractor constraints and palaeoclimate regimes. *Dynamics and Statistics of the Climate System* **2017**, *1*, 1–21.
7. Köhler, P.; Stap, L.B.; von der Heydt, A.S.; de Boer, B.; van de Wal, R.S.W.; Bloch-Johnson, J. A State-Dependent Quantification of Climate Sensitivity Based on Paleodata of the Last 2.1 Million Years. *Paleoceanography* **2017**, *32*, 1102–1114.
8. Dessler, A.E.; Forster, O.M. An estimate of equilibrium climate sensitivity from interannual variability. *Journal of Geophysical Research - Atmospheres* **2018**, *123*.
9. Cox, P.M.; Huntingford, C.; Williamson, M. Emergent constraint on equilibrium climate sensitivity from global temperature variability. *Nature* **2018**, *553*, 319–322.
10. Rypdal, M.; Fredriksen, H.B.; Rypdal, K.; Steene, R.J. Emergent constraints on climate sensitivity. *Nature* **2018**, pp. doi: 10.1038/s41586-018-0639-4.
11. Fredriksen, H.B.; Rypdal, M. Long-range persistence in global surface temperatures explained by linear multibox energy balance models. *Journal of Climate* **2017**, *30*, 7157 – 7168.
12. Myhre, G.; Myhre, C.L.; Forster, P.M.; Shine, K.P. Halfway to doubling of CO₂ radiative forcing. *Nature Geoscience* **2017**, *10*, 710–711.

13. Andrews, T.; Gregory, J.M.; Webb, M.J.; Taylor, K.E. Forcing, feedbacks and climate sensitivity in CMIP5 coupled atmosphere-ocean climate models. *Geophysical Research Letters* **2017**, *39*, L09712.
14. Forster, P.M.; Andrews, T.; Good, P.; Gregory, J.M.; Jackson, L.S.; Zelinka, M. Evaluating adjusted forcing and model spread for historical and future scenarios in the CMIP5 generation of climate models. *Journal of Geophysical Research - Atmospheres* **2013**, *118*, 1139–1150.
15. Hansen, J.; Sato, M.; Kharecha, P.; von Schuckmann, K.; Beerling, D.J.; Cao, J.; Marcott, S.; Masson-Delmotte, V.; Prather, M.J.; Rohling, E.J.; Shakun, J.; Smith, P.; Lacy, A.; Russell, G.; Ruedy, R. Young people's burden: requirement of negative CO₂ emissions. *Earth System Dynamics* **2017**, *8*, 577–616.
16. Rypdal, M.; Rypdal, K. Long-memory effects in linear response models of Earth's temperature and implications for future global warming. *Journal of Climate* **2014**, *27*, 5240–5258.
17. Rypdal, M.; Rypdal, K. Late Quaternary temperature variability described as abrupt transitions on a 1/f noise background. *Earth System Dynamics* **2016**, *7*, 281–293.
18. Rybski, D.; Bunde, A.; Havlin, S.; von Storch, H. Long-term persistence in climate and the detection problem. *Geophysical Research Letters* **2006**, *33*, L06718–L06718.
19. Lovejoy, S.; Schertzer, D. *The Weather and Climate: Emergent Laws and Multifractal Cascades*; Cambridge University Press, 2013.
20. Huybers, P.; Curry, W. Links between annual, Milankovitch and continuum temperature variability. *Nature* **2005**, *441*, 329–332.
21. Franzke, C. Long-Range Dependence and Climate Noise Characteristics of Antarctic Temperature Data. *Journal of Climate* **2010**, *23*, 6074–6081.
22. Fredriksen, H.B.; Rypdal, K. Spectral characteristics of instrumental and climate model surface temperatures. *Journal of Climate* **2016**, *29*, 1253–1268.
23. Rypdal, K.; Rypdal, M.; Fredriksen, H.B. Spatiotemporal long-range persistence in earth's temperature field: Analysis of stochastic-diffusive energy balance models. *Journal of Climate* **2015**, *28*, 8379–8395.
24. Rypdal, K. Global temperature response to radiative forcing: Solar cycle versus volcanic eruptions. *Journal of Geophysical Research - Atmospheres* **2012**, *117*, D06115.
25. Mandelbrot, B.; Ness, J. Fractional Brownian motions, fractional noises and applications. *SIAM Review* **1968**, *18*, 1088–1107.
26. Rue, H.; Martino, S.; Chopin, N. Approximate Bayesian inference for latent Gaussian models using integrated nested Laplace approximations (with discussion). *Journal of the Royal Statistical Society, Series B* **2009**, *71*, 319–392.
27. Sørbye, S.H.; Myrvoll-Nilsen, E.; Rue, H. An approximate fractional Gaussian noise model with $\mathcal{O}(n)$ computational cost. *arXiv:1709.06115* **2018**.
28. Myrvoll-Nilsen, E.; Sørbye, S.H.; Rypdal, M.; Fredriksen, H.B.; Rue, H. Method for estimating climate response under scaling assumption. *preprint* **2018**.